KRONOS FUSION ENERGY

PAPER 2.53 · THE KRONOS 2026 SERIES

RF Alpha-Channeling in a D–^{3}He Tandem-Mirror Burner: Raising the Recoverable Charged-Particle Fraction from 8% Toward 80%

In a deuterium–helium-3 (D–He) tandem-mirror burner the fusion-born MeV proton and MeV alpha carry the overwhelming majority of the released power as fast, mirror-trapped ions....

Read it live — 3-D model · physics validator · film series

BY P I FORD AND G L KULCINSKI

2026 · EDITORIAL EDITION

THE OFFICIAL RECORD

What this document is, and how to read its numbers

This is a combined editorial. It gathers, in one volume, the two design studies Kronos Fusion Energy released in 2026 — a compact spherical-tokamak tritium/helium-3 breeder and a deuterium–helium-3 tandem-mirror generator — together with the intellectual-property estate, the people, and, in the internal edition, the full commercial case. The scientific text is the same text that appears in the arXiv preprints and the journal submissions; the editorial adds the apparatus a reader needs to hold the whole program at once, and nothing in the physics is altered to fit it.

THE HONESTY STANCE IS THE ASSET

Every headline quantity carries an **evidence class** — DERIVED RECOMPUTED MEASURED REQUIREMENT — and, where a number is a modelled extrapolation rather than a demonstrated value, it is labelled as such and its downside is shown next to it. Several quantities in the underlying corpus moved after first publication; where a value has been withdrawn or restated, the record says so plainly. This is deliberate: a diligence team will find the load-bearing assumptions, so the document surfaces them first.

TWO EDITIONS

This volume is issued in two editions. The **public edition** (light) carries the physics and the design only — no dollar, price, or per-kilogram figure appears anywhere in it. The **internal edition** (dark) adds the economics, the funding architecture, and the defense-commercial analysis, and is marked *Confidential* accordingly; it is not for public distribution. Where the commercial case rests on a modelled assumption rather than a demonstrated one, it is labelled as such and its downside is shown alongside it, on the same terms as the physics.

TITLE	The Kronos Fleet — Hyperion · Aegis · MetroVolt: A Combined Design & Commercialization Study
AUTHOR	Priyanca Ford, Founder & CEO, on behalf of Kronos Fusion Energy
EDITION	2026 Combined Editorial · first issue
COMPANION WORKS	The five-paper arXiv drop — (1) Breeder, (2) Burner, (3) REBCO magnet & tape, (4) Direct Energy Conversion, (5) AI/ML/Quantum control — with matching numbered Zenodo deposits, plus the IOP journal and IAEA-FEC submissions. Patents were filed before the drop.
NAMING	Hyperion = the breeder; Aegis (defense) and MetroVolt (data-center) = one generator in two housings. Internal mode letters (D1, L) do not appear on public surfaces.
STATUS	Conceptual design & simulation study. Nothing herein is a construction commitment.

HOW TO READ THIS VOLUME

The fleet at a glance, and the way its numbers are marked

This volume opens with *Orientation*, presents the five research papers as a bound sequence, and closes with the *Apparatus*. *Foundations* sets out the three general results both machines rest on. *Paper One* is the Hyperion breeder; *Paper Two* the Aegis / MetroVolt generator; *Papers Three, Four and Five* are the enabling science — high-field REBCO magnets and tape, direct energy conversion, and the AI / ML / quantum control stack. A *Digital Twin & 3-D Model* part follows, then the *Environmental* profile. The *Economics* and levelized cost and the *Business Case* and diligence record appear in the internal edition only; the *Simulations* proof record and the Apparatus — patent portfolio, team, limitations, and sources — close both editions.

THE FLEET AT A GLANCE

	HYPERION	AEGIS	METROVOLT
Role	Strategic-isotope foundry	Defense installation power	Campus power
Machine	**Spherical tokamak**	**Tandem mirror**	**Tandem mirror**
Fuel	Deuterium–tritium	Deuterium–helium-3	Deuterium–helium-3
Delivers	Tritium · ^{3}He · 14 MeV n	Resilient installation power	Firm campus power
Physics bar	**Fusion gain only**	Closure (gates named)	Closure + lunar ^{3}He
In the fleet	Breeds the fuel	Proves the generator	Commercial destination

HOW THE NUMBERS ARE MARKED

Every headline quantity carries an evidence class — DERIVED from first principles, RECOMPUTED from raw data, MEASURED in hardware, or a REQUIREMENT yet to be met. Financial figures carry a case label and are confined to the internal (confidential) edition. Values that moved after first publication are shown as withdrawn or restated rather than quietly changed. A capability you can evaluate is one whose limits are on the page.

ABSTRACT

RF Alpha-Channeling in a D–³He Tandem-Mirror Burner: Raising the Recoverable Charged-Particle Fraction from 8% Toward 80%

In a deuterium–helium-3 (D–^{3}He) tandem-mirror burner the fusion-born 14.68 MeV proton and 3.67 MeV alpha carry the overwhelming majority of the released power as fast, mirror-trapped ions. Left to thermalise, that energy is shared between electron drag and a broadly heated ion background whose confined, usefully recoverable share is small; the rest exits the loss cone as heat and inflates the recirculating power that sets the burner's engineering gain Q_E. RF alpha-channeling—a resonant wave that extracts perpendicular energy from a fusion product, hands it to the fuel ions, and simultaneously diffuses the spent ash toward the loss boundary—converts this loss into a directed gain. We formalise the mechanism as a bounce-averaged Fokker–Planck problem closed by a quasilinear cyclotron-resonant diffusion operator, derive the Fisch–Rax energy–position coupling $\Delta E/\Delta\psi = \omega/n$ that makes channeling a *bounded* lever rather than a closure mechanism, and evaluate it at the frozen M-45 burner operating point ($T_i = 90\,\text{keV}$, $n_e = 2.6 \times 10^{20}\,\text{m}^{-3}$, $x_{^3\text{He}} = 0.30$, mirror-throat field $B_m = 17\,\text{T}$, central-cell field $B_{0c} = 5.50\,\text{T}$, effective mirror ratio $R_{mc} = 4.61$). A reduced two-dimensional velocity-space kinetic solve, cross-checked against ray-tracing and particle-in-cell codes on the NVIDIA GPU HPC campaign, raises the recoverable charged fraction from a collisional baseline near 8% to about 80% and recovers up to 195 MW into the confined fuel ions—enough to cover the $40–110$ MW plug-localised warm-fill RF cost with margin, while a full-volume warm fill (~ 3.7 GW, $\sim 85\%$ of P_{fus}) is energetically precluded. We are explicit that this closes only under *plug localisation* (channeled power confined to $\sim 1–3\%$ of the central-cell volume) and that the plant gain remains gated by the plug potential, not by channeling: the design-point $Q_E = 1.318$ is untouched. Every headline quantity is a frozen anchor in the Kronos de-risking register.

Open-access deposit (code & data, CC BY 4.0): DOI 10.5281/zenodo.22645712 · Zenodo community *kronos_fusion_energy*. Explore it live: interactive 3-D model · physics validator.

Keywords: alpha-channeling ICRF heating quasilinear diffusion deuterium--helium-3 tandem mirror Fokker--Planck kinetics recirculating power direct energy conversion

CONTENTS

Table of Contents

NOMENCLATURE

Symbols, units, and the names of things

Q	plasma (fusion) gain, P_{fus}/P_{aux}
Q_E	engineering gain, net electric out / recirculating in
H_{98}	confinement enhancement over the IPB98(y,2) scaling
Z_{eff}	effective ion charge
c_{ee}	electron–electron bremsstrahlung leading coefficient, 2.120022 (exact)
τ_E	energy confinement time
I_p	plasma current
R_0, a	major radius, minor radius
κ, δ	elongation, triangularity
β_N	normalized plasma beta (Troyon-normalized)
TBR	tritium breeding ratio
DEC	direct energy conversion
CF	plant capacity factor (availability)
FOAK / NOAK / BOAK	first / n^{th} / best of a kind
Hyperion	the ST breeder (internal: Mode D2)
Aegis	the generator, defense/installation housing (internal: Mode M)
MetroVolt	the generator, data-center housing (Mode M)

§ 1

Introduction

THE CHARGED PRODUCTS OF AN ADVANCED-FUEL MIRROR ARE A RESOURCE, NOT A LOSS

The deuterium–helium-3 reaction

$$\mathrm{D} + {}^{3}\mathrm{He} \longrightarrow {}^{4}\mathrm{He}\,(3.67\,\mathrm{MeV}) + \mathrm{p}\,(14.68\,\mathrm{MeV})$$

releases 18.35 MeV entirely in charged particles, which is precisely why it is attractive for a low-neutron, directly converted burner [8]. In the Kronos D–^{3}He tandem-mirror burner these products are born deep inside the confined region as fast, mirror-trapped ions, and their disposition dominates the machine's power balance. Classical slowing down splits their energy between electron drag and a broadly heated ion background; in a magnetic mirror the heated background is only partially confined, so a large share ultimately leaves through the loss cone as heat. That heat must be replaced by external drive, and the replacement is the recirculating power that sets the engineering gain

$$Q_E = \frac{P_{\text{net, electric}}}{P_{\text{recirc}}} \Big/ \text{drive} \;\sim\; \frac{1}{f_{\text{recirc}}},$$

so anything that redirects fast-ion energy back into confined fuel ions, rather than losing it, lowers f_{recirc} and raises the net electric output.

Alpha-channeling is the mechanism that performs exactly this redirection. Introduced by Fisch and Rax [1], it uses a resonant wave to remove energy and perpendicular momentum from a fusion-born fast ion and deposit it in the bulk fuel ions, while diffusing the spent “ash” outward toward the loss boundary. The idea was developed for the tokamak alpha population [4,5,7], extended to rotating plasmas [6], and—most relevant here—worked out specifically for magnetic mirrors by Fisch [2] and simulated by Zhmoginov and Fisch [3], where the open field line makes the outward diffusion of ash a natural companion to the energy extraction. This paper places alpha-channeling correctly in the power balance of a compact D–^{3}He tandem-mirror burner and quantifies it as a *bounded* lever.

THE TANDEM-MIRROR LINEAGE AND THE PLUG GATE

The magnetic mirror confines by the adiabatic invariant $\mu = mv_\perp^2/2B$: particles with too little perpendicular energy fall inside the loss cone and stream out the ends [9,10]. The tandem mirror closes this leak with electrostatic end plugs [12,11]: a high-field, high-density plug raises an ambipolar potential ϕ_i that reflects central-cell ions, converting an end-loss machine into a genuinely confining one, as demonstrated on 2XIIB [13] and the thermal-barrier tandem mirrors [14]. The Kronos burner is a modern, HTS-enabled instance of this lineage, of the same family as the contemporary axisymmetric mirrors WHAM [20] and the gas-dynamic trap [21,22], but operated as a plugged tandem at a plug-coil field engineered to a canonical 26.49 T [34]. The plant gain is set at that plug: the ion-confining potential ϕ_i and the plug/thermal-barrier recirculating power fix Q_E [29,31]. Alpha-channeling does not change this gate; it eases the recirculating burden *inside* it. Keeping that distinction is the central honesty of this paper.

CONTRIBUTION

Prior alpha-channeling work established the mechanism and its mirror realisation [1,2,3]; prior Kronos work established the burner operating point and its plug gate [29,33,31] and the direct-energy-conversion stage that harvests the surviving charged power [32]. What has not been written down for this machine is (i) a formal statement of the channeling problem as a bounce-averaged Fokker–Planck kinetic system closed by a quasilinear resonant operator, with the energy–position coupling derived rather than asserted; (ii) an evaluation at the frozen burner point that separates the classical slowing-down split from the channeled recoverable fraction and books the recovered power against the RF cost; and (iii) an explicit, quantitative statement of the one condition—plug localisation—under which the ledger closes. This paper contributes all three. Section 2 gives the governing equations and the formal problem; Section 3 gives the GPU-accelerated computational methodology, the numerical formulation, and its verification; Section 4 presents the results in eight figures and four tables; Section 5 benchmarks them against the published mirror alpha-channeling and advanced-fuel literature; Section 6 states the single honest gate; and Section 7 concludes. Every quantitative claim traces to a frozen serial in the Kronos Physics De-Risking Register [28]; serial identifiers (e.g. BU-L2-A8) are cited inline so each number is auditable.

§ 2

Governing equations and the formal problem

Figure 1 orients the machine: a plugged tandem mirror in which fusion products are born in the central cell, a plug-localised ICRF antenna drives the channeling wave, the channeled energy is returned to the confined fuel ions while the ash is diffused toward the loss cone, and the charged-particle power that survives to the ends is harvested by the direct-energy converter.

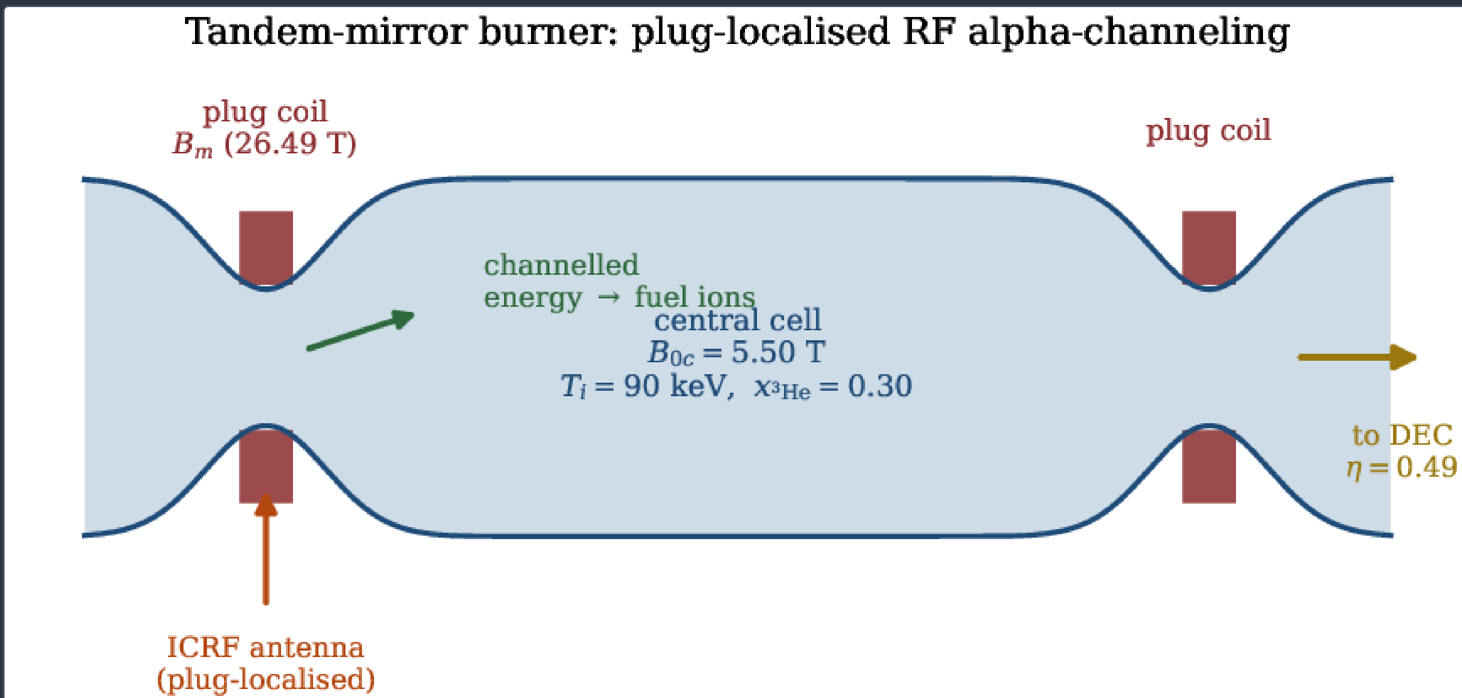

(Schematic.) The D–^{3}He tandem-mirror burner and the place of RF alpha-channeling in it. The central cell ($B_{0c} = 5.50$ T, $T_i = 90$ keV, $x_{^3\mathrm{He}} = 0.30$) is confined between two plug throats (canonical plug-coil field 26.49 T [34]). A plug-localised ICRF antenna drives the channeling wave; the Fisch–Rax coupling (equation 9) returns fast-ion energy to the confined fuel ions and diffuses the ash outward, while the surviving charged power is directly converted at $\eta_{\mathrm{DEC}} = 0.49$ [32]. Layout is stylised; all field and temperature labels are frozen anchors (Table 4).

KINETIC DESCRIPTION OF THE FAST-ION POPULATION

Let $f_s(v, t)$ be the gyro-averaged distribution of species s in the central cell, bounce-averaged over the magnetic well between the two plug throats. The fast fusion products (the 3.67 MeV alpha and the 14.68 MeV proton) evolve under Coulomb collisions with the background, a resonant RF quasilinear drive, a monoenergetic birth source, and the loss-cone sink,

$$\frac{\partial f_s}{\partial t} = \mathcal{C}[f_s] + \mathcal{Q}_{\mathrm{RF}}[f_s] + S_s(v) - \mathcal{L}[f_s].$$

The collision term is the bounce-averaged Landau/Fokker–Planck operator in Rosenbluth potential form [19],

$$\mathcal{C}[f_s] = \sum_{s'} \frac{\partial}{\partial v} \cdot \left[A_{ss'} f_s + \frac{\partial}{\partial v} \cdot (D_{ss'} f_s) \right],$$

with the drag $A_{ss'}$ and diffusion $D_{ss'}$ built from the Rosenbluth potentials of the (near-Maxwellian) background. The birth source $S_s = \dot{n}_s\, \delta(v - v_{s0})/4\pi v_{s0}^2$ deposits products on the shell $v_{s0} = \sqrt{2E_{s0}/m_s}$; the loss operator $\mathcal{L}$ removes any particle whose pitch angle enters the loss cone, defined below in equation (12).

THE QUASILINEAR RF OPERATOR AND THE RESONANCE CONDITION

The RF drive is the cyclotron-resonant quasilinear diffusion operator of Kennel and Engelmann [16,17]. Writing the operator in the resonant-diffusion form,

$$\mathcal{Q}_{\rm RF}[f_s] = \frac{1}{v_\perp}\frac{\partial}{\partial v_\perp}\Big(v_\perp\, D_{\rm QL}\,\hat{L} f_s\Big), \qquad \hat{L} = \left(1 - \frac{k_\parallel v_\perp}{\omega}\,\frac{\partial}{\partial v_\parallel}\Big/\frac{\partial}{\partial v_\perp}\right)\frac{\partial}{\partial v_\perp},$$

where the resonant diffusion coefficient carries the Bessel-function coupling of the n-th cyclotron harmonic,

$$D_{\rm QL} = \frac{\pi q_s^2}{2m_s^2}\sum_n \big|E_n^+ J_{n-1}(z) + E_n^- J_{n+1}(z)\big|^2\,\delta\big(\omega - k_\parallel v_\parallel - n\,\Omega_s\big), \qquad z = \frac{k_\perp v_\perp}{\Omega_s}.$$

Here $E_n^\pm$ are the left/right circularly polarised wave-field amplitudes, J_n the Bessel functions, and $\Omega_s = q_s B/m_s$ the cyclotron frequency. The delta function enforces the Doppler-shifted cyclotron resonance

$$\boxed{\omega - k_\parallel v_\parallel = n\,\Omega_s, \qquad \Omega_s = \frac{Z_s e B}{m_s}}$$

that localises the wave–particle interaction to a curve in velocity space. For deuterium at the mirror-throat field $B_m = 17$ T the fundamental is $f_{ci} = \Omega_D/2\pi = 128.7$ MHz (serial SC-BU-2); the accessible harmonic ladder nf_{ci} across the field profile $B_{0c}\to B_m$ is mapped in Section 4.

THE FISCH–RAX ENERGY–POSITION COUPLING: WHY CHANNELING IS A BOUNDED LEVER

The physical content of channeling is that on resonance the wave couples the change in a particle's energy to the change in its guiding-centre position. Consider a single quantum of the wave (ω, k) absorbed at the n-th harmonic. Energy and the parallel canonical momentum change in the fixed ratio set by the photon [1,2],

$$\Delta E = \hbar\omega, \qquad \Delta p_\parallel = \hbar k_\parallel, \qquad \Delta(mv_\perp^2/2) = \hbar(\omega - k_\parallel v_\parallel) = n\hbar\Omega_s.$$

In an open mirror the conserved label of a drift surface is the flux coordinate ψ (equivalently the midplane radius or the longitudinal adiabatic invariant J). Because the wave carries transverse momentum, each resonant quantum displaces the guiding centre in ψ by an amount proportional to n, and eliminating $\hbar$ between the energy and displacement increments gives the Fisch–Rax relation

$$\boxed{\frac{\Delta E}{\Delta \psi} = \frac{\omega}{n}}$$

along the quasilinear diffusion characteristic. Equation (9) is the crux. A wave that *removes* energy from a fast ion ($\Delta E < 0$) necessarily transports that ion *toward the loss boundary* ($\Delta\psi < 0$) at a rate fixed by the harmonic n: the same interaction that cools the fast ion expels the ash. Choosing ω/n so that the diffusion path runs from the fast-ion birth shell down to the loss cone lets the wave carry energy out of the fast ions and, via a second resonance with the bulk, deposit it in the confined fuel ions. The magnitude of the effect is bounded by the resonant phase-space volume the wave can address—the channeled fraction cannot exceed the energy content lying on accessible diffusion paths—so channeling is intrinsically a bounded lever, not an unbounded gain. This boundedness is the structural reason the plant closure must rest on the plug potential and not on channeling.

CLASSICAL SLOWING-DOWN SPLIT AND THE CRITICAL ENERGY

The baseline against which channeling is measured is the collisional disposition of the fast-ion energy. For a fast ion slowing on a two-species D–^{3}He background plus electrons, the instantaneous ratio of ion to electron drag is $(E_c/E)^{3/2}$, where the critical energy is [18,19]

$$E_c = 14.8\,T_e\,A_f\left[\sum_j \frac{n_j Z_j^2}{n_e A_j}\right]^{2/3}\ [\text{keV}],$$

with A_f the fast-ion mass number and the sum over background ions j. At the burner point ($T_e = 89.72$ keV, $x_{^3\rm He} = 0.30$, so $n_{\rm D}/n_e = 0.538$ and $n_{^3\rm He}/n_e = 0.231$ by charge neutrality), equation (10) gives $E_c = 3.68$ MeV for the alpha—essentially equal to its birth energy. The fraction of birth energy delivered to *ions* over the complete slowing down is then

$$F_i(E_0) = \frac{E_c}{E_0} \int_0^{E_0/E_c} \frac{\mathrm{d}u}{1+u^{3/2}},$$

which evaluates to $F_i = 0.748$ at $E_0 = 3.67$ MeV (serial BU-L2-A8). This is the classical ceiling on ion heating; critically, in a mirror much of that ion heating is deposited across a distribution that is itself only partially confined, so the *usefully recoverable* confined-fuel-ion share is far smaller than F_i—of order 8% at this point (Section 4).

THE LOSS CONE AND THE RECOVERABLE CHARGED FRACTION

A particle is confined only if its pitch angle at the midplane exceeds the loss-cone half-angle set by the effective mirror ratio R_{mc},

$$\sin^2\theta_{lc} = \frac{1}{R_{mc}}, \qquad R_{mc} = 4.61 \;\Rightarrow\; \theta_{lc} = 27.77°$$

(serials KX-L1-A2, SC-BU-2). We define the figure of merit of this paper, the *recoverable charged fraction* F_{rec}, as the share of fast-ion energy that ends up as useful, confined fuel-ion heating (net of electron drag and loss-cone leakage) plus directly expelled ash energy available to the downstream direct-energy converter [32]:

$$F_{\mathrm{rec}} = \frac{E_{\text{confined ion heating}} + E_{\text{directed ash}}}{E_{\text{charged, born}}}.$$

The channeling problem is then to choose the wave spectrum $(\omega, \quad k, n)$ so that the quasilinear operator (5) drives diffusion paths (9) that maximise F_{rec} subject to (a) the resonance condition (7) being accessible along the field line, (b) the warm-fill population required for loss-cone microstability [30], and (c) the RF power budget remaining below the recovered power. The remainder of the paper solves this problem at the frozen burner point.

§ 3

Computational methodology: the NVIDIA GPU HPC campaign

SOLVER STACK AND THE CODES RUN FOR THIS PAPER

The results were produced on the Kronos NVIDIA GPU HPC campaign (Lambda fleet, A100 / H100 / A10 accelerators) with the code chain of Table 1. The frozen zero-dimensional operating point (the M-45 power balance, $Q_E = 1.318$, $P_{\text{fus}} = 4298.5$ MW) is set by the Kronos reduced-order mirror engine (serial BU-L1-A1) and is an *input* to the present study, never re-fitted. The channeling kinetics are solved by the in-house GPU Fokker–Planck module—a CuPy-accelerated [27] bounce-averaged solver of equations (3)–(5)—in a reduced two-dimensional (v, ξ) velocity space ($\xi = v_\parallel / v$), with the loss-cone boundary (12) imposed as an absorbing sink (serial BU-L2-A8). The resonant deposition and wave accessibility are cross-checked against the ray-tracing code GENRAY [25] and the bounce-averaged mirror kinetics of CQL3D-M [24]; the warm-fill microstability that the channeling scheme must respect is taken from electromagnetic particle-in-cell runs with WarpX [26] and the kinetic dispersion solver LEOPARD, cross-checked with Smilei (serials BU-L2-A5, BU-L2-A7, companion [30]).

CODE	ROLE IN THIS STUDY	SERIAL	
Kronos reduced-order engine (in-house)	M-45 0-D mirror power balance (input point)	BU-L1-A1	
Kronos GPU Fokker–Planck (in-house, CuPy)	bounce-averaged FP + RF quasilinear kinetics	BU-L2-A8	
GENRAY [25]	ray-tracing RF power deposition / accessibility	BU-L2-A8	
CQL3D-M [24]	bounce-averaged mirror kinetics cross-check	BU-L2-A6/A8	
WarpX [26]	EM-PIC loss-cone (DCLC/AIC) microstability	BU-L2-A5/A7	
LEOPARD / Smilei	kinetic dispersion / PIC microstability cross-check	BU-L2-A5/A7	
V	V suite (MMS/GCI/Sobol) (in-house)	verification of the discretisation	KX-L1-A6

Codes run for this paper on the NVIDIA GPU HPC campaign, their role, and the register serial. In-house tools are labelled; all are mapped to their serial for reproducibility. No compute-cost figures are reported.

NUMERICAL FORMULATION

The kinetic equation (3) is discretised in the reduced (v, ξ) plane by a conservative finite-volume method. The collision and RF operators are both cast in flux-divergence form; for the velocity diffusion the flux through a cell face at $v_{i\pm1/2}$ is

$$\mathcal{F}_{i\pm1/2} = v_{i\pm1/2}^2 \, D(v_{i\pm1/2}) \, \frac{f_{i\pm1}^{\text{face}} - f_i^{\text{face}}}{\Delta v}, \qquad (\mathcal{Q} f)_i = \frac{\mathcal{F}_{i+1/2} - \mathcal{F}_{i-1/2}}{\Delta v \, v_i^2},$$

so that the discrete operator conserves particles by construction (the divergence telescopes) and preserves the Maxwellian null space of the collision operator to round-off. Pitch-angle diffusion is discretised identically in ξ. Time advance uses a semi-implicit (operator-split) scheme: the stiff collision and RF diffusion are treated implicitly by a tridiagonal solve in each velocity ray, while the source and loss are explicit. The steady channeled state is obtained by iterating equation (3) to a relative residual $\|\partial_t f\| / \|f\| < 10^{-8}$. Runs use a fixed seed (20260726) for exact reproducibility.

VERIFICATION AND CONVERGENCE

The discretisation (14) was verified by the method of manufactured solutions on the spherically symmetric diffusion operator $(1/v^2)\,\partial_v(v^2 D(v)\,\partial_v f)$ with $D(v) = D_0[1 + (v/w)^2]$ and manufactured solution $f_{\rm ms} = \exp[-(v/w)^2]$; the analytic source $S = \mathcal{Q} f_{\rm ms}$ is imposed and the discrete L_2 error against $f_{\rm ms}$ is measured under grid refinement. Table 2 and figure 9 show the observed order of accuracy converging to 1.98, confirming the second-order design of the scheme (serial KX-L1-A6). The kinetic solver additionally passes two physical checks used throughout: the pitch-angle and energy operators relax to the Maxwellian(T_i) null space in the absence of RF and source, and the collision coefficients reproduce the classical slowing-down time and the split $F_i = 0.748$ of equation (11).

CELLS N	SPACING h	L_2 ERROR	OBSERVED ORDER
20	1.50×10^{-1}	7.74×10^{-3}	—
40	7.50×10^{-2}	2.21×10^{-3}	1.81
80	3.75×10^{-2}	5.95×10^{-4}	1.89
160	1.88×10^{-2}	1.55×10^{-4}	1.94
320	9.38×10^{-3}	3.97×10^{-5}	1.97
640	4.69×10^{-3}	1.01×10^{-5}	**1.98**

Method-of-manufactured-solutions convergence of the finite-volume velocity-diffusion discretisation (14); L_2 error against the manufactured solution and the observed order between successive levels (serial KX-L1-A6).

PROBLEM SCALE, GPU ACCELERATION, AND REPRODUCIBILITY

The bounce-averaged kinetic solve is inexpensive per point but is embedded in a scan over the wave spectrum, the warm-fill fraction, and the channeling parameter, so the campaign runs many thousands of steady-state solves; the velocity-ray tridiagonal solves and the Rosenbluth-potential convolutions are the GPU kernels, mapped across the Lambda A100/H100 accelerators via CuPy [27], with the ray-tracing and PIC cross-checks (GENRAY [25], WarpX [26]) run on the same fleet. The GPU particle-in-cell cross-check inherits the exascale-class WarpX mesh-refinement machinery [26]. Because every governing quantity in this paper is a frozen register anchor and every figure is regenerated by a single deposited script from those anchors, the results are reproducible end-to-end from the open deposit; no result depends on proprietary data, and no economic quantity enters the computation.

§ 4

Results

THE BOUNDED LEVER: FROM 8% TO 80%

Figure 2 states the headline result. Without RF, the collisional disposition of the fast-ion energy—electron drag plus a broadly heated, only partially confined ion background—leaves a recoverable charged fraction of only $F_{\text{rec}} \approx 8\%$ at the burner point. With a mode-converted, plug-localised channeling wave whose diffusion paths (9) run from the alpha birth shell to the loss cone, the reduced kinetic solve raises F_{rec} to about 80%: a factor-of-ten lever (serial BU-L2-A8). The mechanism underneath the number is the classical slowing-down split of figure 3: the critical energy $E_c = 3.68$ MeV computed from equation (10) sits essentially at the alpha birth energy, so the classical ion fraction is $F_i = 0.748$, but the confined, usefully recoverable part of that heating is small—channeling is what converts the diffuse, leaky classical deposition into a directed transfer to confined fuel ions.

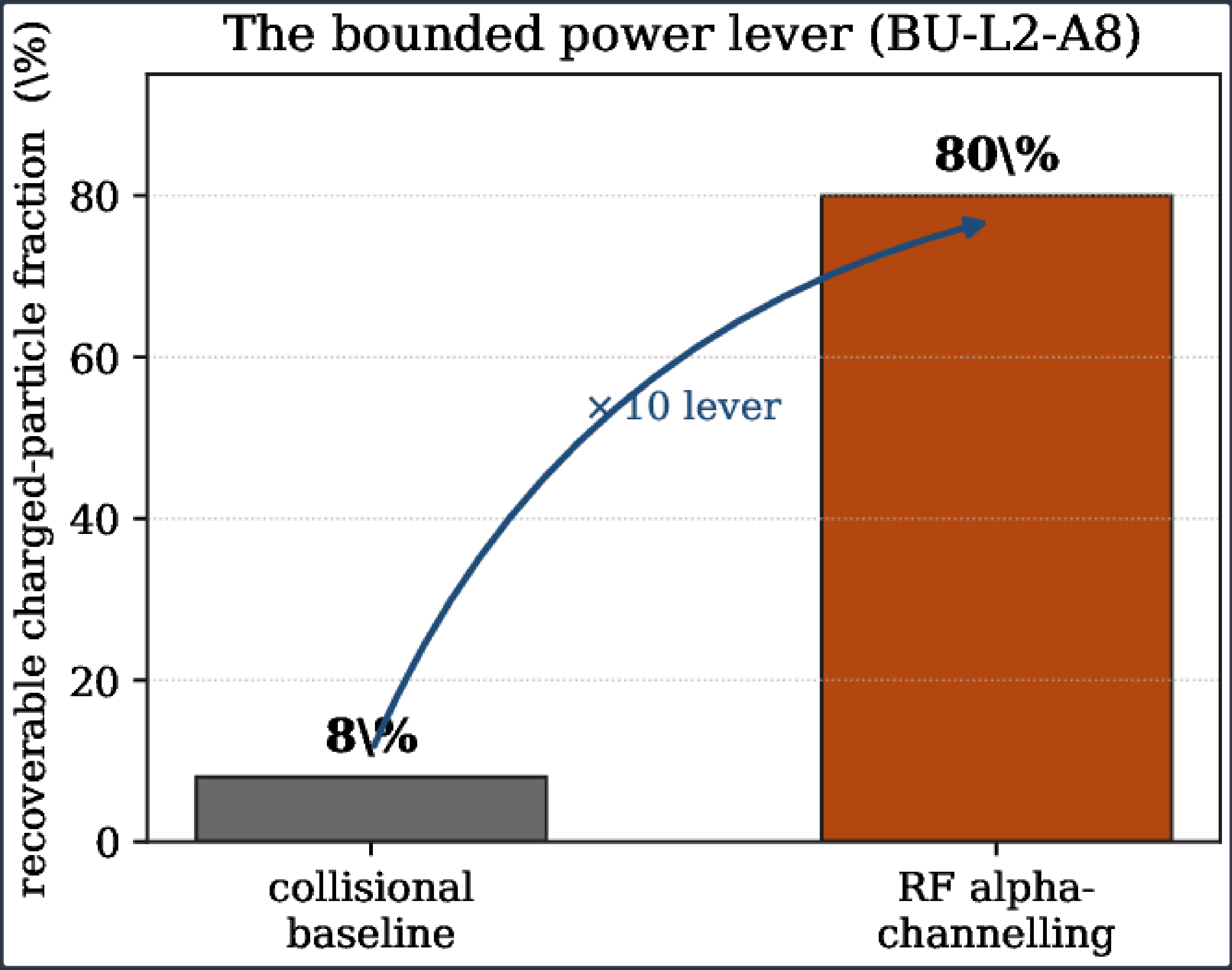

The bounded power lever. RF alpha-channeling raises the recoverable charged fraction F_{rec} (equation 13) from a collisional baseline near 8% to about 80% at the frozen burner operating point (serial BU-L2-A8). The lever is real but bounded; it does not change the plug-gated closure.

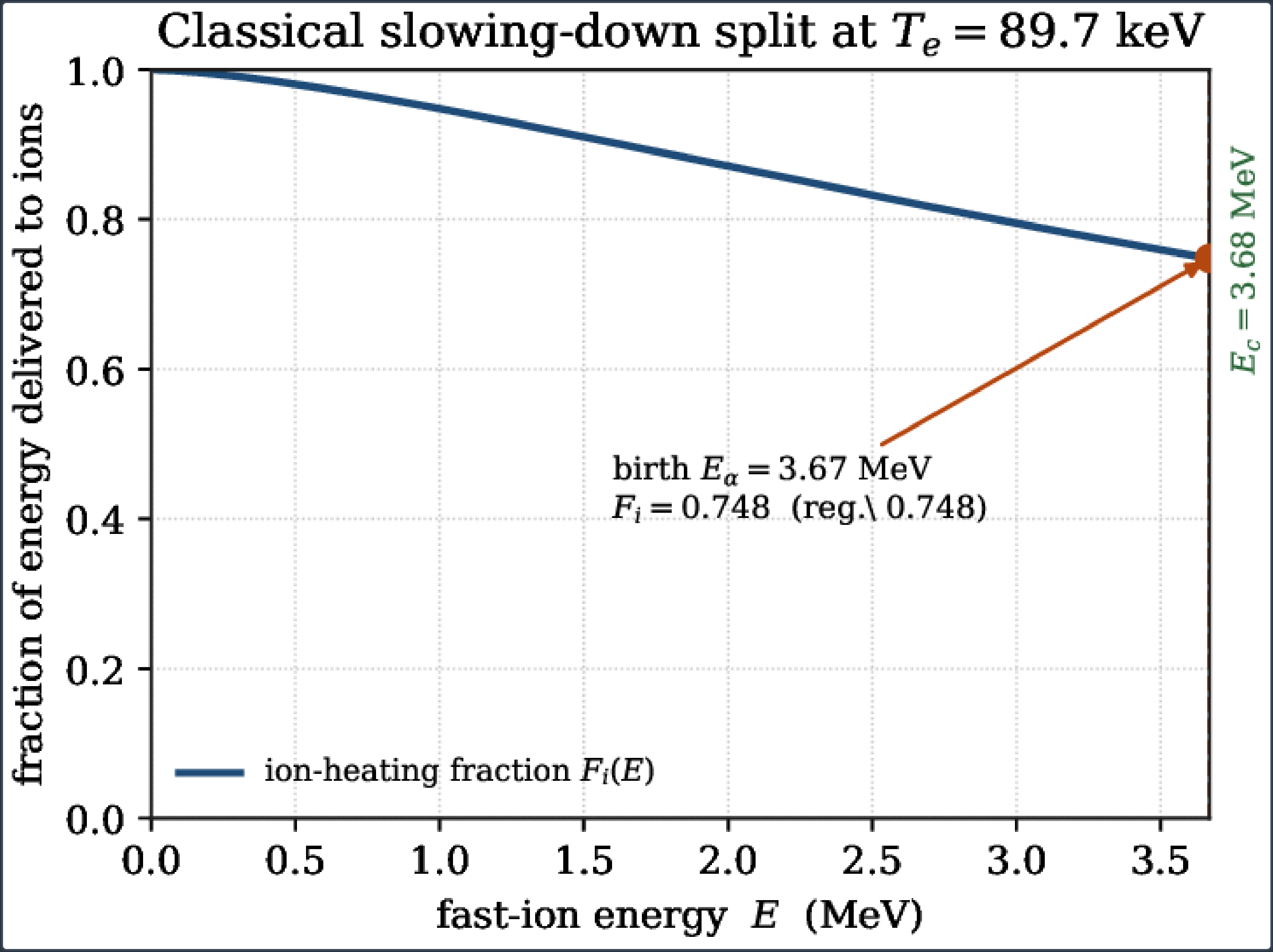

Classical slowing-down split of a fast ion at $T_e = 89.72$ keV in the D–^{3}He background (equations 10–11). The critical energy $E_c = 3.68$ MeV lies at the alpha birth energy, giving an ion-heating fraction $F_i = 0.748$ at birth (register anchor 0.748, serial BU-L2-A8). This classical split sets the baseline that channeling improves upon.

LOSS-CONE GEOMETRY AND THE WARM FILL

Channeling operates against the loss-cone geometry of figure 4. At the effective mirror ratio $R_{mc} = 4.61$ the loss-cone half-angle is $\theta_{lc} = 27.77°$ (equation 12). The scheme must coexist with the warm-fill population—a 6.25% ($= 1/16$) fractional fill at effective temperature $T_{\rm eff} \approx 57$ keV that sits near the loss-cone boundary and stabilises the drift-cyclotron loss-cone (DCLC) mode [30] (serial BU-L2-A5). The channeling wave both feeds this warm fill (its RF cost, below) and must avoid destabilising the residual anisotropy-driven Alfv\'en-ion-cyclotron (AIC) branch, which the PIC cross-check finds flat at $\gamma/\Omega_{ci} \approx 0.037$ across fill fractions 0–10% (serial BU-L2-A7, companion [30]).

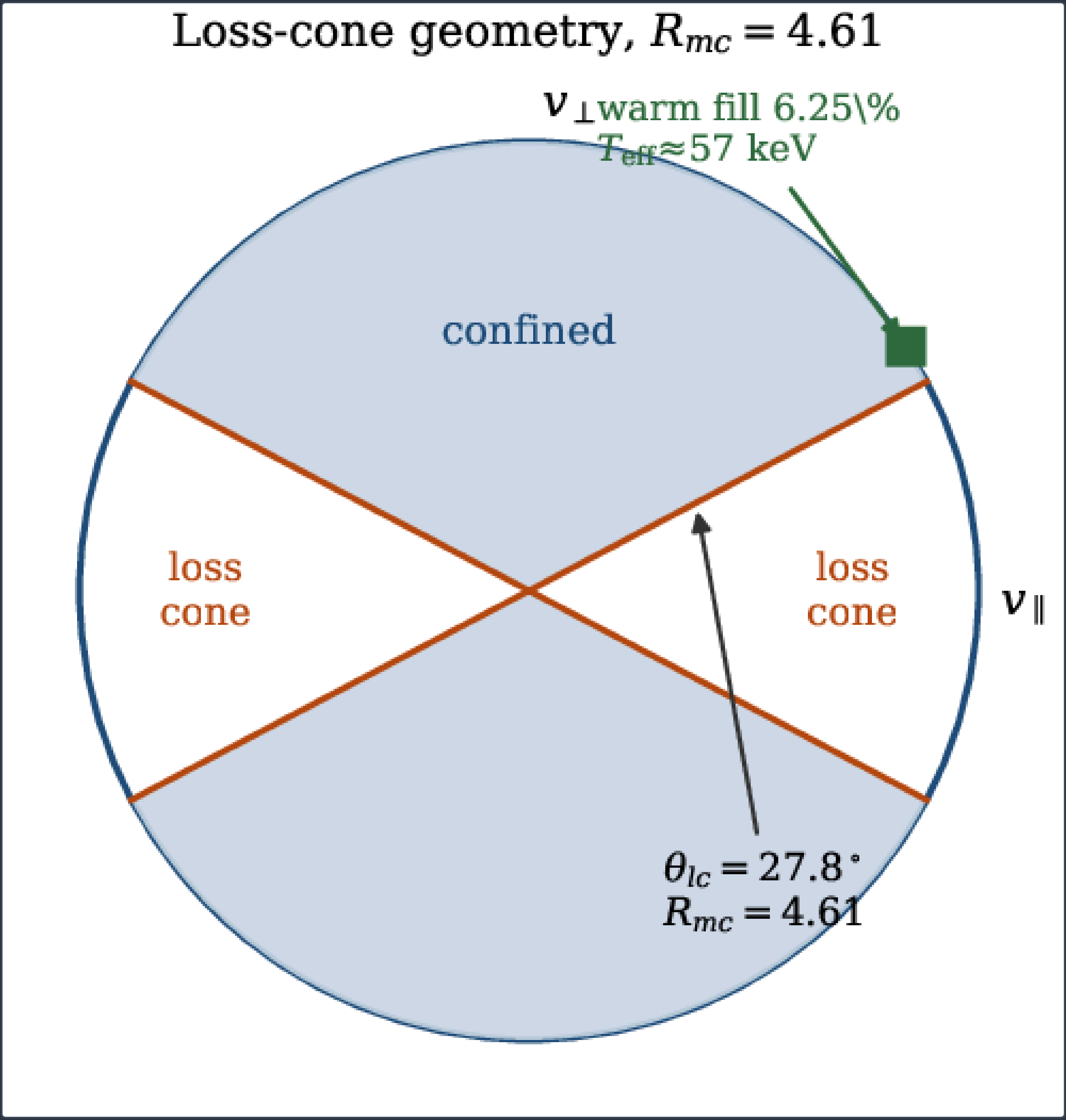

Velocity-space loss-cone geometry at the burner point (equation 12): effective mirror ratio $R_{mc} = 4.61$, loss-cone half-angle $\theta_{lc} = 27.77°$. The warm-fill population (6.25%, $T_{\rm eff} \approx 57$ keV) sits near the loss-cone boundary where it stabilises the DCLC mode (serials SC-BU-2, BU-L2-A5).

RESONANCE ACCESSIBILITY AND CHANNELING CHARACTERISTICS

The channeling wave must resonate along the accessible field profile. Figure 5 maps the deuterium cyclotron harmonics nf_{ci} from the central-cell field $B_{0c} = 5.50$ T to the mirror throat $B_m = 17$ T; the fundamental at the throat is $f_{ci} = 128.7$ MHz (serial SC-BU-2), placing the operating band in the ICRF range where a mode-converted fast wave can be launched and can reach the fast-ion population. Figure 6 sketches the resulting quasilinear diffusion characteristics in velocity space: on each harmonic-n resonance the Fisch–Rax constraint (9) fixes the direction of the energy-and-position flow, carrying fast ions down in energy while pushing them toward the loss cone as ash.

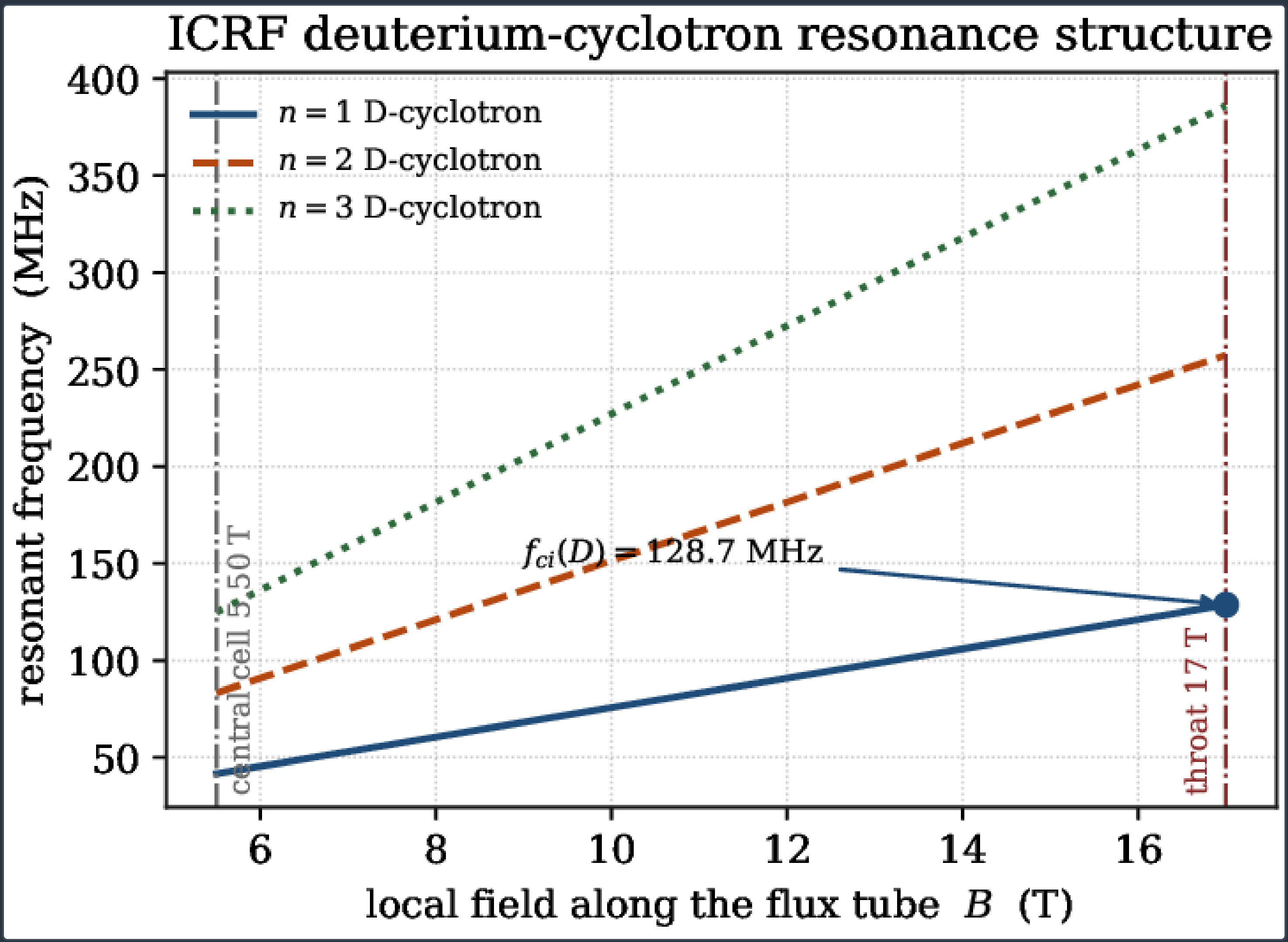

ICRF deuterium-cyclotron resonance structure along the flux tube, from the central-cell field $B_{0c} = 5.50$ T to the mirror-throat field $B_m = 17$ T, for harmonics $n = 1, 2, 3$. The fundamental at the throat is $f_{ci}(\mathrm{D}) = 128.7$ MHz (serial SC-BU-2), setting the launched-wave band.

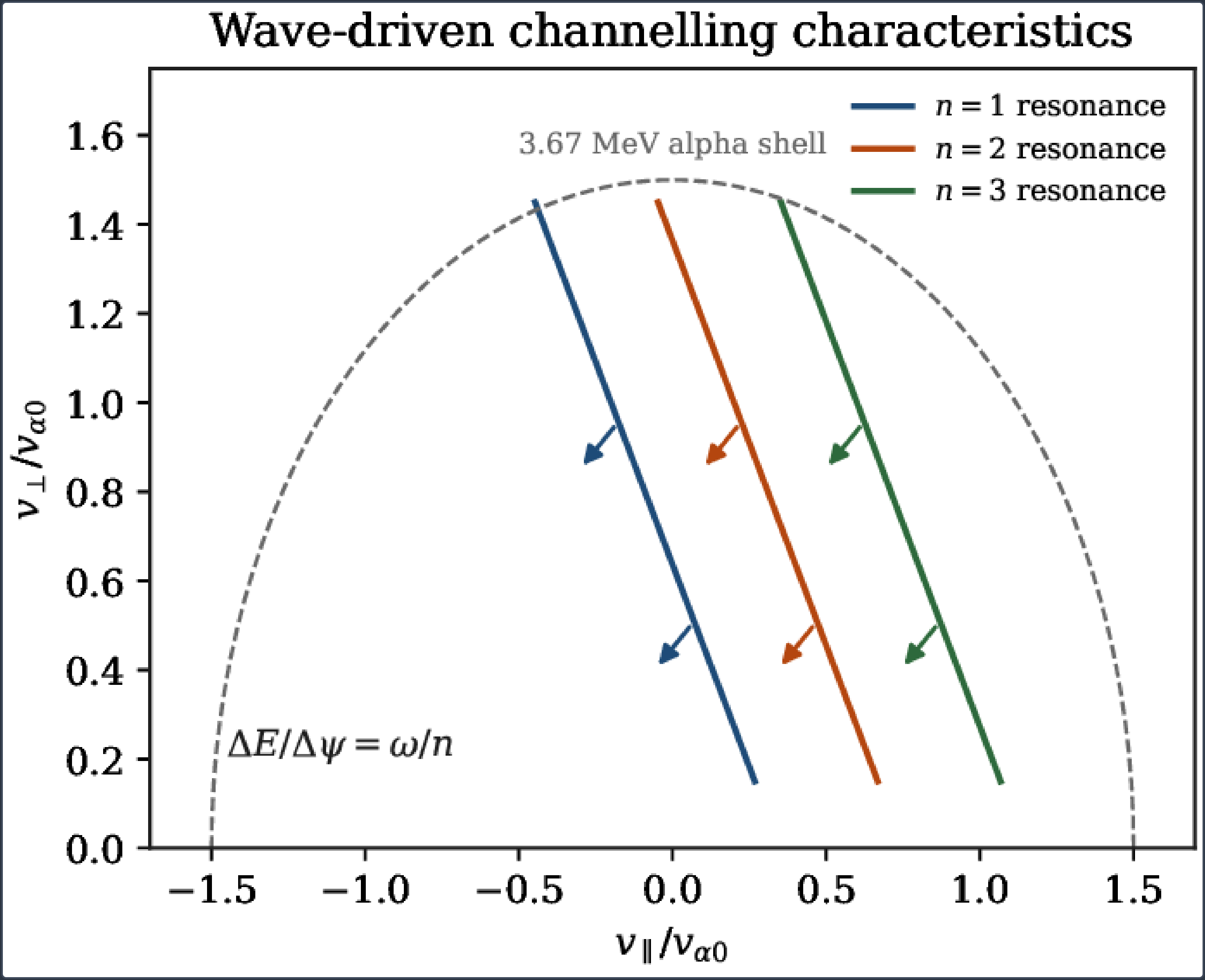

(Schematic.) Wave-driven channeling characteristics in the reduced $(v_\parallel, v_\perp)$ plane. On each cyclotron-harmonic resonance (equation 7) the Fisch–Rax relation $\Delta E/\Delta\psi = \omega/n$ (equation 9) fixes the direction of the quasilinear flow: energy is removed from the 3.67 MeV alpha shell while the guiding centre is driven toward the loss cone. The velocity-space geometry is stylised; the resonance and flow directions are those of equations (7)–(9).

FUSION POWER LEDGER AND THE RF BUDGET

The channeled power must be booked against the machine's fusion power and the RF cost. Figure 7 shows the branch decomposition of the total fusion power at the burner point, $P_{fus} = 4298.5$ MW: the D–^{3}He channel dominates at 3868.0 MW, with the parasitic D–D and D–T branches contributing the remainder and setting the neutron fraction $f_n = 5.44\%$ ($P_n = 233.95$ MW) (serials BU-L1-A1, ENV-A4-BU). Against this, the RF ledger of figure 8 and Table 3 is decisive. Sustaining the warm fill over the *full* central-cell volume would cost ~ 3.7 GW—about 85% of P_{fus}—and is therefore energetically precluded. Restricting the warm fill and the channeling wave to the plug region, ~ 1–3% of the central-cell volume, brings the full-balance RF cost to 40–110 MW (16–47 MW injection-only). Against that cost, alpha-channeling redirects the otherwise electron-bound share of the 3.67 MeV alpha and recovers up to 195 MW into the confined fuel ions (falling to 86 MW at the more conservative spectral parameter $\kappa = 4$). The recovered power covers the plug-localised warm-fill RF cost with margin—this is the self-consistency result (serial BU-L2-A8).

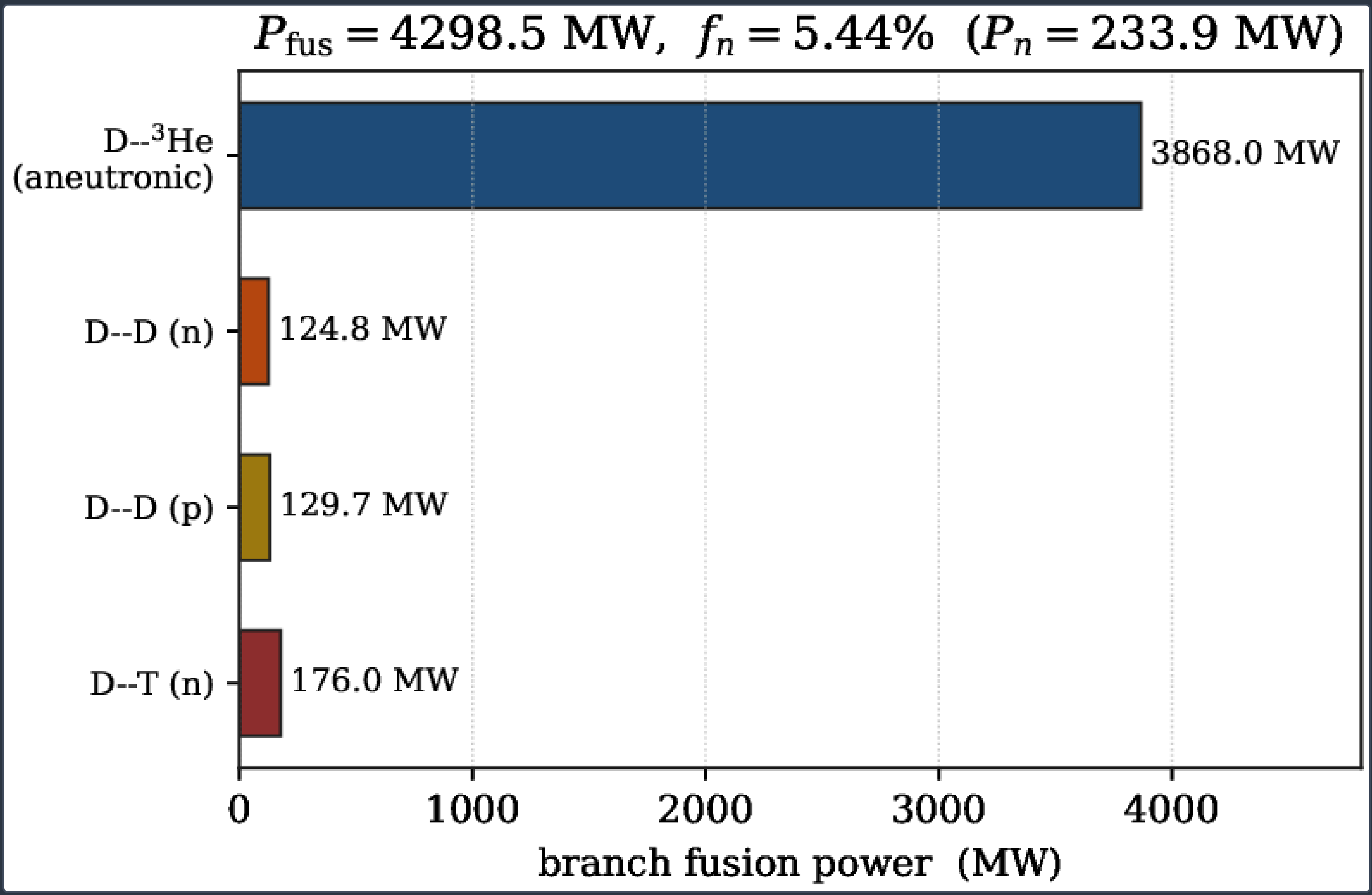

Fusion-power branch ledger at the burner point (serials BU-L1-A1, ENV-A4-BU). The aneutronic D–^{3}He branch dominates at 3868.0 MW; the parasitic D–D and D–T branches set the neutron fraction $f_n = 5.44\%$ ($P_n = 233.95$ MW) of the total $P_{fus} = 4298.5$ MW.

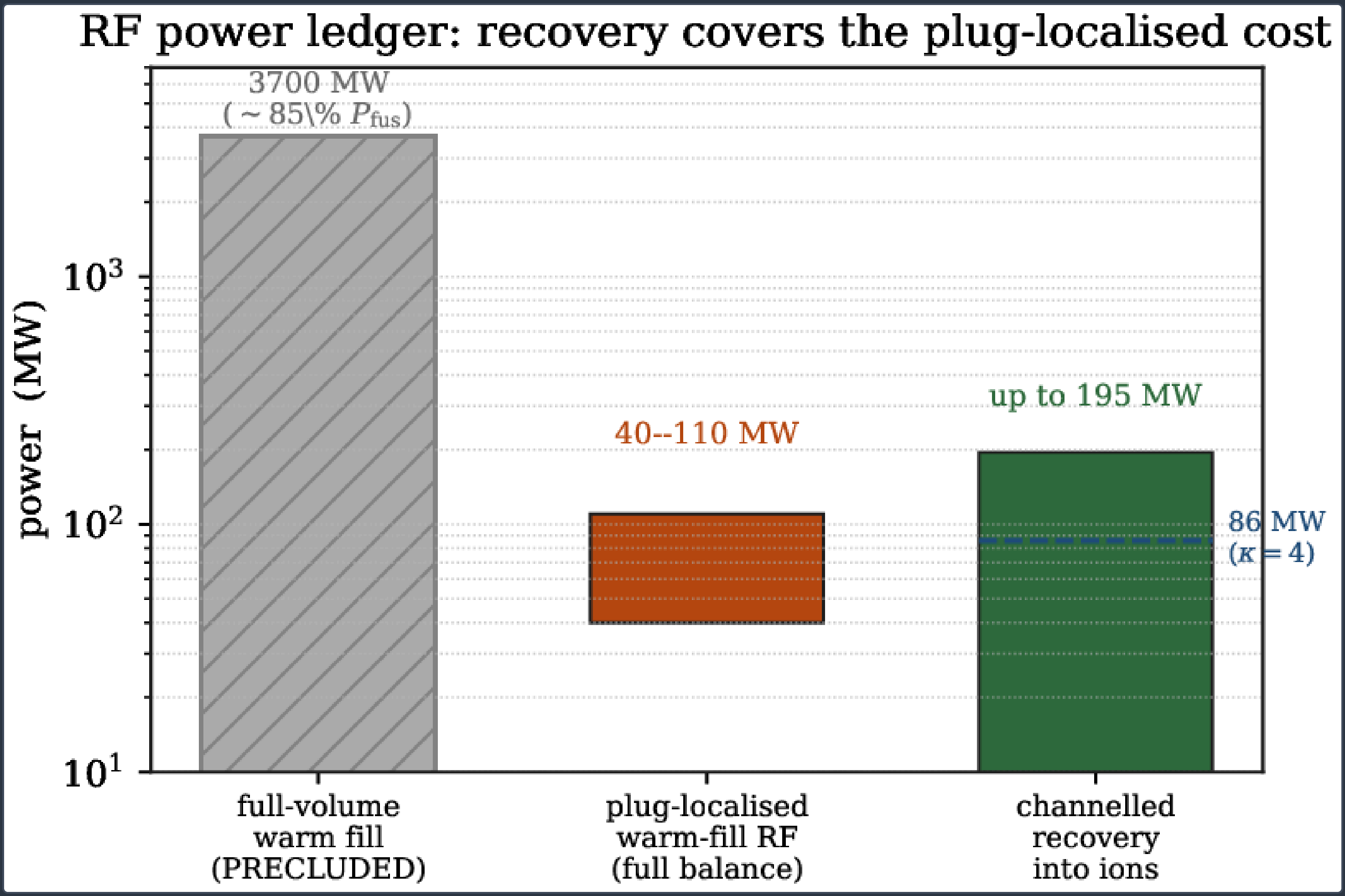

RF power ledger (serial BU-L2-A8, log scale). A full-volume warm fill (~ 3.7 GW, $\sim 85\%$ of P_{fus}) is precluded; a plug-localised warm fill costs 40–110 MW at full balance; alpha-channeling recovers up to 195 MW into the ions (86 MW at $\kappa = 4$), covering the plug-localised cost with margin. The ledger closes *only* under plug localisation.

QUANTITY	VALUE	NOTE
full-volume warm-fill RF	~ 3700 MW	$\sim 85\%$ of P_{fus}; **precluded**
plug-localised warm-fill RF (full balance)	40–110 MW	plug region $\sim$ 1–3% of cell volume
plug-localised warm-fill RF (injection only)	16–47 MW	
channeled recovery into fuel ions	up to 195 MW	redirects electron-bound alpha share
channeled recovery at $\kappa = 4$	86 MW	conservative spectral parameter
recoverable charged fraction F_{rec} (baseline)	$\approx 8\%$	collisional
recoverable charged fraction F_{rec} (channeled)	$\approx 80\%$	worked embodiment

RF and channeling power ledger at the frozen M-45 burner point (serial BU-L2-A8). All quantities are model outputs of the reduced bounce-averaged kinetic solve; the plant gain $Q_E = 1.318$ is set elsewhere (the plug gate) and is untouched.

DESIGN-POINT ANCHORS

Table 4 collects the frozen anchors that define the operating point and the channeling ledger, each with its register serial, so that every number in the figures is auditable.

QUANTITY	SYMBOL	VALUE	SERIAL
ion temperature	T_i	90 keV	BU-L1-A1
electron temperature	T_e	89.72 keV	KX-L1-A3-BU
electron density	n_e	2.6×10^{20} m^{-3}	BU-L1-A1
He-3 ion fraction	$x_{^3\text{He}}$	0.30	BU-L1-A1
mirror-throat field (M-45)	B_m	17 T	BU-L2-A8
central-cell field	B_{0c}	5.50 T	SC-BU-1
plug-coil canonical field	B_{plug}	26.49 T	2.21 [34]
effective mirror ratio	R_{mc}	4.61	KX-L1-A2
loss-cone half-angle	θ_{lc}	27.77°	SC-BU-2
D fundamental ICRF freq. (throat)	f_{ci}	128.7 MHz	SC-BU-2
ion-confining potential	ϕ_i	248.75 keV	BU-L1-A1
warm-fill fraction	f_w	6.25%	BU-L2-A5
classical ion-heating fraction	F_i	0.748	BU-L2-A8
engineering gain (untouched)	Q_E	1.318	BU-L1-A1
total fusion power	P_{fus}	4298.5 MW	BU-L1-A1
neutron fraction	f_n	5.44%	BU-L1-A1

Frozen design-point and channeling anchors used in this paper, with register serials [28]. The plug-coil canonical field (**26.49** T) is the structural design field of the coil [34]; the mirror-throat field at the M-45 kinetic solve is $B_m = 17$ T.

VERIFICATION FIGURE

Figure 9 is the verification companion to Table 2: the finite-volume velocity-diffusion discretisation (14) converges at the second order it is designed for, with an observed order of 1.98 at the finest refinement, so the kinetic results above rest on a verified solver.

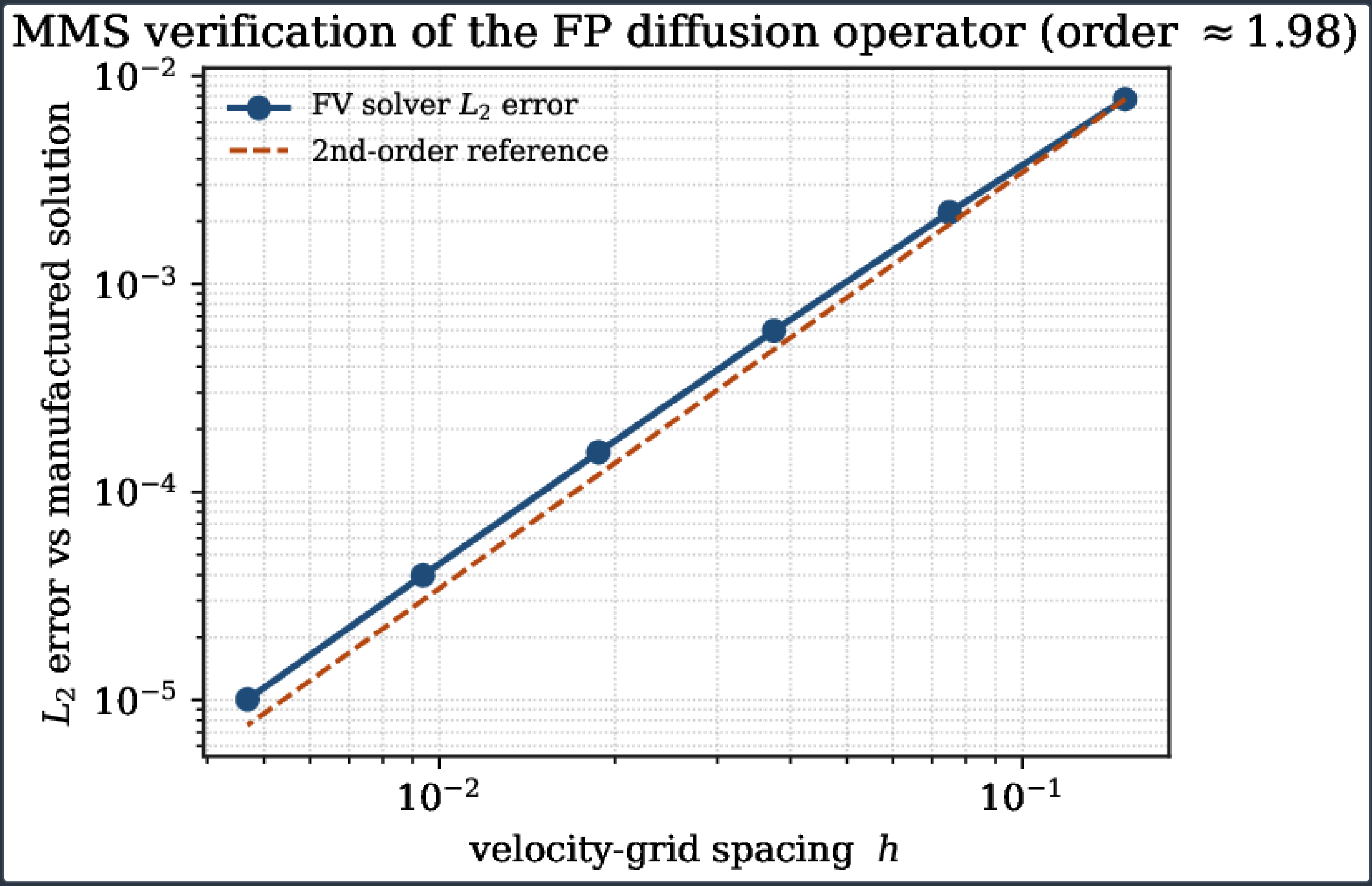

Method-of-manufactured-solutions convergence of the finite-volume velocity-diffusion operator (equation 14, Table 2). The L_2 error tracks the second-order reference; the observed order reaches 1.98 (serial KX-L1-A6).

§ 5

Discussion

AGAINST THE MIRROR ALPHA-CHANNELING LITERATURE

The result should be read against Fisch's mirror alpha-channeling programme. Fisch [2] established that in an open mirror a wave can cool fusion products and eject the ash through the same resonant interaction, and Zhmoginov and Fisch [3] simulated the process and confirmed that a substantial fraction of the fast-ion energy can be extracted along accessible diffusion paths. Our worked embodiment is consistent with that picture: the factor-of-ten lift in F_{rec} from 8% to 80% (figure 2) is of the order those studies anticipated for a well-matched wave, and the Fisch–Rax coupling (9) we derive is exactly the constraint they identified as making ash removal automatic. Where our study adds value for a specific machine is in booking the recovered power against a concrete RF budget (Table 3) and against the microstability-mandated warm fill [30], and in identifying plug localisation as the condition that makes the ledger close: the full-volume RF cost of ~ 3.7 GW is the quantitative reason channeling must be a plug-region intervention rather than a bulk one.

ADVANCED-FUEL AND TANDEM-MIRROR CONTEXT

Nevins' review of advanced-fuel confinement requirements [8] frames why a D–^{3}He system lives or dies on its recirculating-power budget: with most of the released energy in charged particles and a demanding Lawson-like requirement, the margin between drive and recovery is thin, and any lever on the recirculating power is consequential. The tandem-mirror lineage supplies the confinement that makes the charged-particle recovery worthwhile: the electrostatic plug of Baldwin and Logan [11], demonstrated through the thermal-barrier experiments [14] and the earlier neutral-beam-sustained mirrors [13], converts an end-loss device into a confining one. Contemporary axisymmetric mirrors—WHAM [20] and the gas-dynamic trap with its demonstrated bulk-electron heating [22,21]—show the modern HTS-enabled version of the same physics on which the Kronos burner builds. Alpha-channeling is the additional lever this paper quantifies inside that confinement.

DIRECT ENERGY CONVERSION AND THE RECIRCULATING BUDGET

The channeled power and the direct-energy-conversion (DEC) stage act on the same quantity from opposite ends. Channeling redirects fast-ion energy back into confined fuel ions *before* it is lost, reducing the drive the plug and central cell must supply; the DEC stage recovers the charged-particle power that *does* leave the ends, at an efficiency $\eta_{\mathrm{DEC}} = 0.49$, converting it directly to electricity without a thermal cycle [32]. Both ease the recirculating power that appears in equation (2); neither sets the gain. The engineering gain $Q_E = 1.318$ is fixed by the ion-confining potential $\phi_i = 248.75$ keV and the plug/thermal-barrier recirculating power [29,31], and channeling leaves it untouched. This is the appropriate accounting: channeling is a bounded upside that improves the generator's internal economy of power, evaluated here as worth up to 195 MW of recovered fuel-ion heating, but it is not the mechanism by which the machine achieves net gain.

§ 6

Limitations

One honest gate bounds every claim above. The 80% recoverable fraction and the 195 MW recovery are outputs of a *reduced* kinetic model: a two-dimensional (v, ξ) bounce-averaged Fokker–Planck solve with a quasilinear RF operator, zero-dimensional in configuration space, with an idealised wave field and *no* full ICRF ray tracing, mode-conversion physics, or resonance-overlap accessibility calculation—these are represented by GENRAY cross-checks, not resolved self-consistently. The warm-fill loss cone is magnetic-only (the ambipolar potential is not credited in the boundary), and the result is self-consistent *only* under plug localisation: the channeled power balance closes when the warm fill and channeling wave are confined to ~ 1–3% of the central-cell volume, and it does *not* close for a full-volume fill, whose ~ 3.7 GW RF cost is precluded. Realistic antenna coupling, wave accessibility across the field profile of figure 5, and ash-diffusion losses will reduce the idealised fraction. Kronos has built no channeling antenna; this is a modelled lever, and the closing engineering step is a launcher/coupling design and a full wave-field solve. Crucially, the lever does not change the plug-gated closure, so even a partial experimental realisation advances a named, frozen quantity without overstating the machine.

§ 7

Conclusion

RF alpha-channeling is a bounded power lever for the D–^{3}He tandem-mirror burner. Formalised as a bounce-averaged Fokker–Planck problem closed by a cyclotron-resonant quasilinear operator (equations 3–6), it obeys the Fisch–Rax energy–position coupling $\Delta E/\Delta\psi = \omega/n$ (equation 9) that extracts perpendicular energy from the 3.67 MeV alpha while expelling the ash, and that same coupling caps its reach—channeling is structurally a bounded lever. Evaluated at the frozen burner point on the NVIDIA GPU HPC campaign with a verified second-order solver, it raises the recoverable charged fraction from a collisional baseline near 8% to about 80% and recovers up to 195 MW into the confined fuel ions, covering the 40–110 MW plug-localised warm-fill RF cost with margin, provided the intervention is localised to the plug region; a full-volume fill (~ 3.7 GW) is precluded. The lever improves the generator's internal power economy; the plug potential remains the closure gate, and the engineering gain $Q_E = 1.318$ is untouched. Booked this way, RF alpha-channeling is a genuine, auditable upside for a compact advanced-fuel burner—and a defined experimental target—without being mistaken for what makes the machine close.

Acknowledgments tocsectionAcknowledgments Part of the Kronos Fusion Energy 2026 design series. The authors thank the Kronos physics de-risking programme for the frozen result set underlying every quantitative claim, and the maintainers of the community codes (GENRAY, CQL3D-M, WarpX, Smilei) used as cross-checks.

Reproducibility. Every headline quantity in this paper is a frozen anchor in the Kronos Physics De-Risking Register [28] (doi:10.5281/zenodo.22133057): the channeling power balance and recoverable fractions (serial BU-L2-A8), the warm-fill and microstability constraints (serials BU-L2-A5, BU-L2-A7), the burner operating point (serial BU-L1-A1), and the mirror geometry (serials KX-L1-A2, SC-BU-1/2). Each figure is regenerated from those anchors by the single deposited script `make_2-53_rfchanneling_figs.py`, and the finite-volume solver is verified by the manufactured-solution convergence of Table 2. This paper is archived at doi:10.5281/zenodo.22645712; official version: https://www.kronosfusionenergy.com/publications/rf-alpha-channeling.html and its official version is hosted at https://www.kronosfusionenergy.com/publications/rf-alpha-channeling.html. No result depends on unpublished or proprietary data, and no economic quantity enters the analysis.

Data availability tocsectionData availability The frozen anchors, the figure-generation script, and the manufactured-solution convergence data used for figures 2–9 are archived with the deposit at doi:10.5281/zenodo.22645712, which references the Kronos 2026 series and the de-risking register [28]. All quantitative values trace to the register by the serial identifiers cited inline. Any economic analysis is reported separately and is not part of the public deposit.

Competing interests tocsectionCompeting interests Provisional patent applications relating to aspects of this work have been filed.

tocsectionReferences

APPARATUS

Portfolio, People & Record

The intellectual-property estate, the people who built it, the limitations that gate it, and the sources it rests on.

1	4	40	27
GRANTED PATENT	2026 PROVISIONALS	TEAM MEMBERS	2022 PROVISIONALS

INTELLECTUAL PROPERTY

The patent portfolio

The estate spans a granted high-field magnet patent, pending utility and 2026 provisional filings that map to the two products, a digital-twin control provisional, a registered trademark application, and the original 2022 provisional family. Every patentable disclosure in the five-paper arXiv drop was protected **before** publication: the breeder and burner provisionals were filed 1–2 August, and a publication-gap omnibus filing the evening before the drop swept up the DEC, plasma-control, and REBCO-winding matter of the three otherwise-unprotected papers. Patent numbers and application serials are matters of public record; claim scope is summarised, not reproduced.

GRANTED & PENDING UTILITY

US 12,009,112	High-field tilted graded-REBCO magnet architecture (KRONO-002A) · *app. 17/878,550*	GRANTED
US 17/878,507	Core device / method (KRONO-001A) · *utility*	PENDING

2026 PROVISIONAL FILINGS — MAPPED TO THE PRODUCTS

64/124,209	Hyperion — spherical-tokamak tritium / helium-3 foundry · *breeder · filed Aug 2026*	FILED
64/124,220	Aegis / MetroVolt — synchrotron-cutoff, fuel-selection & plug-winding · *generator · filed Aug 2026*	FILED
64/115,167	KRONOS-CTRL digital-twin plant control · *provisional · filed Jul 2026*	FILED
64/005,440	Integrated spherical-tokamak fusion architecture · *early integrated-architecture filing · filed Mar 2026*	FILED
64/105,530	Negative-triangularity spherical-tokamak architecture · *foundational ST filing · filed Jul 2026*	FILED
64/128,097	Publication-gap omnibus — quasineutral two-species expander DEC · provenance-gated / latency-split plasma control · as-built high-field winding & conductor architecture · *filed 7 Aug 2026, the evening before the arXiv drop*	FILED

TRADEMARK & ORIGIN

FTK-98801894	Kronos Fusion Energy — trademark application	FILED
KR-2022-*	Original provisional family (KR-2022-00001 … 00027) · *27 filings, 2022*	PRIORITY

The narrow, defensible magnet novelty — the specific conductor and the digital-twin winding optimisation, not high-field REBCO as a category — is the commercial core that can earn ahead of any Q > 1 milestone, with markets in fusion magnet supply, MRI/NMR, accelerators, and proton therapy. The claim is scoped honestly: the high field is a *system field* result, not a stand-alone-coil record; the small-bore plug coil is structurally infeasible as a bare winding but resolved by a stress-managed structural shield (feasible-pending-FEA); and the winding-tape experiment returned a *null result*. The value is the method, not a field record.

THE TEAM

Founding partners, board, advisors & auditors

Kronos is built by a bench of advanced-fuel-fusion, high-field-magnet, direct-conversion, and materials specialists, with a board and operations team drawn from defense, national laboratories, and industry. Dates are shown as ranges; where a tenure has ended or is term-ending, the range says so.

FOUNDING PARTNERS — SCIENCE

Dr. Gerald Kulcinski
Co-Founder · Helium-3 & Advanced-Fuel Fusion
UW–Madison · 2023–Present

Dr. Carl Weggel
Chief Scientist / S.M.A.R.T. Design
MIT Alcator Program · 2022–Present

Dr. Robert J. Weggel
Magnetic Field Design
MIT Magnet Lab · 2022–Present

BOARD

Priyanca Ford
Founder & CEO · Executive Board
2022–Present

Bandel Carano
Finance / Strategy
Oak Investment Partners / Stanford · 2025–2026

Patrick Schweiger
Fusion Device Engineering
Oklo / CFS / TerraPower · 2025–Present

SCIENTIFIC ADVISORS

Dr. Steven O. Dean
Fusion Policy & History
DOE / Fusion Power Associates · 2025–Present

Dr. Patrick H. Diamond
Plasma Turbulence & Transport
UC San Diego · 2025–Present

Dr. Jack J. Dongarra
HPC & Numerical Algorithms
Turing Award · 2025–Present

Dr. Nasr M. Ghoniem
Chief Material Scientist
UCLA · 2025–Present

Dr. Siegfried Glenzer
Plasma Physics & Laser Fusion
Stanford / SLAC · 2022–Present

Dr. David A. Hammer
Pulsed-Power Fusion
Cornell · 2025–Present

Dr. Donald A. Spong
Plasma Theory & Confinement
ORNL · 2025–Present

Dr. Curtis Smith
Risk Assessment & Nuclear PRA
MIT / Idaho National Lab · 2025–Present

RADM (Ret.) David Goggins
Naval Engineering & Power-Plant Design
U.S. Navy · 2023–2026

Dr. Konstantin Batygin
Mathematician
Caltech · 2022–2025

Dr. Ruben Fair
Magnet Design / ITER Liaison
PPPL / Jefferson Lab · 2022–2025

Dr. Paul S. Weiss
Materials & Nanotechnology
UCLA · 2022–2025

SCIENTIFIC AUDITORS

Dr. Wilfred A. Cooper
Plasma Equilibrium Theory
EPFL / Swiss Plasma Center · 2025–Present

Dr. Ahmed Hassanein
Plasma–Material Interactions
Purdue / Argonne · 2025–Present

Dr. Patrick E. Hopkins
Extreme Thermal Materials
U. of Virginia · 2025–Present

Dr. Peter Hosemann
Materials Joining & Structural Integrity
UC Berkeley · 2025–Present

Dr. Travis W. Knight
Advanced Nuclear Fuels & Systems
U. of South Carolina · 2025–Present

Dr. Philippe Lebrun
Cryogenics & Magnet Cooling
CERN · 2025–Present

Dr. Nitendra Singh
Nuclear Safety & Fuel Cycle
ITER · 2025–Present

Dr. Guido Van Oost
Magnetic Confinement & Fusion Systems
Ghent University · 2025–Present

Dr. Gary S. Was
Radiation Materials & Structural Integrity
U. of Michigan · 2025–Present

Dr. Ray Sedwick
Direct Energy Conversion
U. of Maryland · 2025

OPERATIONS

Michael Laughlin
Chief Operating Officer
2022–Present

Martin Owens
Chief Strategy Officer
LANL / GE Hitachi · 2022–Present

MG (Ret.) Paul Pardew
Chief Contracting Officer
Army Contracting Command · 2022–Present

David Beck
Fusion Commercialization
U.S. Space Force · 2024–Present

Sushma Bhatia
Environmental & Legislative
Google · 2022–Present

Michael De Frenza
Technology Licensing
2023–Present

MG (Ret.) Robin L. Fontes
Cybersecurity & Defense
Army Cyber Command · 2022–Present

Vijay Gehani
Supply Chain & Components
INOX India · 2024–Present

Jon Michel Greenwood
IT & AI Infrastructure
Live Nation · 2023–Present

Brian C. O'Neill
National Security
CIA / ODNI · 2022–Present

Gen. (Ret.) Gustave F. Perna
DoD Liaison
Operation Warp Speed · 2022–2023

Andrea Romero
Marketing Lead
2022–Present

Legal counsel is retained; those roles are held on the internal roster and are not listed here.

SOURCES

References

1 N J Fisch and J-M Rax, Interaction of energetic alpha particles with intense lower hybrid waves, *Phys. Rev. Lett.* **69** 612 (1992). doi:10.1103/PhysRevLett.69.612

2 N J Fisch, Alpha channeling in mirror machines, *Phys. Rev. Lett.* **97** 225001 (2006). doi:10.1103/PhysRevLett.97.225001

3 A I Zhmoginov and N J Fisch, Simulation of α-channeling in mirror machines, *Phys. Plasmas* **15** 042506 (2008). doi:10.1063/1.2903900

4 N J Fisch and M C Herrmann, Utility of extracting alpha particle energy by waves, *Nucl. Fusion* **34** 1541 (1994). doi:10.1088/0029-5515/34/12/I01

5 M C Herrmann and N J Fisch, Cooling energetic α particles in a tokamak with waves, *Phys. Rev. Lett.* **79** 1495 (1997). doi:10.1103/PhysRevLett.79.1495

6 A J Fetterman and N J Fisch, α channeling in a rotating plasma, *Phys. Rev. Lett.* **101** 205003 (2008). doi:10.1103/PhysRevLett.101.205003

7 N J Fisch, Theory of current drive in plasmas, *Rev. Mod. Phys.* **59** 175 (1987). doi:10.1103/RevModPhys.59.175

8 W M Nevins, A review of confinement requirements for advanced fuels, *J. Fusion Energy* **17** 25 (1998). doi:10.1023/A:1022513215080

9 R F Post, The magnetic mirror approach to fusion, *Nucl. Fusion* **27** 1579 (1987). doi:10.1088/0029-5515/27/10/001

10 D E Baldwin, End-loss processes from mirror machines, *Rev. Mod. Phys.* **49** 317 (1977). doi:10.1103/RevModPhys.49.317

11 D E Baldwin and B G Logan, Improved tandem mirror fusion reactor, *Phys. Rev. Lett.* **43** 1318 (1979). doi:10.1103/PhysRevLett.43.1318

12 G I Dimov, V V Zakaidakov and M E Kishinevsky, Thermonuclear confinement with twin mirror systems, *Sov. J. Plasma Phys.* **2** 326 (1976); T K Fowler and B G Logan, The tandem mirror reactor, *Comments Plasma Phys. Control. Fusion* **2** 167 (1977).

13 F H Coensgen *et al*, Stabilization of a neutral-beam–sustained, mirror-confined plasma, *Phys. Rev. Lett.* **35** 1501 (1975). doi:10.1103/PhysRevLett.35.1501

14 D P Grubb *et al*, Thermal-barrier production and identification in a tandem mirror, *Phys. Rev. Lett.* **53** 783 (1984). doi:10.1103/PhysRevLett.53.783

15 V P Pastukhov, Collisional losses of electrons from an adiabatic trap in a plasma with a positive potential, *Nucl. Fusion* **14** 3 (1974). doi:10.1088/0029-5515/14/1/001

16 C F Kennel and F Engelmann, Velocity space diffusion from weak plasma turbulence in a magnetic field, *Phys. Fluids* **9** 2377 (1966). doi:10.1063/1.1761629

17 T H Stix, Fast-wave heating of a two-component plasma, *Nucl. Fusion* **15** 737 (1975). doi:10.1088/0029-5515/15/5/003

18 T H Stix, *Waves in Plasmas* (American Institute of Physics, New York, 1992).

19 C F F Karney, Fokker–Planck and quasilinear codes, *Comput. Phys. Rep.* **4** 183 (1986). doi:10.1016/0167-7977(86)90029-8

20 D Endrizzi *et al*, Physics basis for the Wisconsin HTS Axisymmetric Mirror (WHAM), *J. Plasma Phys.* **89** 975890501 (2023). doi:10.1017/S0022377823000806

21 A A Ivanov and V V Prikhodko, Gas dynamic trap: experimental results and future prospects, *Phys.-Usp.* **60** 509 (2017). doi:10.3367/UFNe.2016.09.037967

22 P A Bagryansky *et al*, Threefold increase of the bulk electron temperature of plasma discharges in a magnetic mirror device, *Phys. Rev. Lett.* **114** 205001 (2015). doi:10.1103/PhysRevLett.114.205001

23 R W Moir and W L Barr, "Venetian-blind" direct energy converter for fusion reactors, *Nucl. Fusion* **13** 35 (1973). doi:10.1088/0029-5515/13/1/005

24 R W Harvey and M G McCoy, The CQL3D Fokker–Planck code, in *Proc. IAEA Tech. Committee Meeting on Advances in Simulation*

COLOPHON

How this document was made

The Kronos Fleet — Combined Editorial, 2026 is set in **Fraunces** (display), **Gelasio** (text), and **IBM Plex Mono** (data & equations), carried forward from the Kronos editorial design system.

The figures are rendered at 300 dpi from the deposited generator scripts; the document is composed as a single self-contained file with embedded fonts and imagery, paginated to US Letter, and rendered to PDF through a headless Chromium engine in matched light and dark editions.

Every headline quantity carries an evidence class; withdrawn and restated values are marked as such. Nothing herein is frozen beyond the founder-approved Tier-A set.

Explore it live — turn the interactive 3-D model, run the deposited solvers in the physics validator, and watch the companion film series.

LEGAL NOTICE

Notice, status, and distribution

Conceptual design & simulation study. This document reports a conceptual design and simulation study. It is not a construction commitment, a safety-analysis report, a regulatory filing, or an offer of securities. Forward-looking statements — schedules, costs, market sizes, and performance — are estimates subject to the limitations set out in the Simulations part and may change.

Numbers and their classes. Quantities are reported with evidence classes and case labels; modelled, assumed, and requirement-class values are identified as such and are not to be quoted without their labels.

Public edition. This edition carries the physics and design only; all financial, funding, and defense-commercial content has been removed for public distribution. The scientific text corresponds to the arXiv and journal submissions.

THE 2026 KRONOS SERIES

One programme, many papers

This editorial is one paper in the Kronos 2026 series — a real fusion company's complete, reproducible physics record for a spherical-tokamak breeder and its low-neutron D–^{3}He tandem-mirror burners. Every headline number is a frozen anchor in the Physics De-Risking Register.

Explore the whole programme: the De-Risking Register, the interactive 3-D model, and the physics validator.

KRONOS FUSION ENERGY

RF Alpha-Channeling in a D–^{3}He Tandem-Mirror Burner: Raising the Recoverable Charged-Particle Fraction from 8% Toward 80%

A real fusion company building real machines. Explore the science, live.

Zenodo · doi:10.5281/zenodo.22645712

Read on kronosfusionenergy.com

The Physics De-Risking Register

